Research report

Ventromedial prefrontal cortex damage alters resting blood flow to the bed nucleus of stria terminalis

CrossMark

Julian C. Motzkin [a,b,c], *Carissa L. Philippi* [a], *Jonathan A. Oler* [a],
Ned H. Kalin [a], *Mustafa K. Baskaya* [d] *and Michael Koenigs* [a,*]

[a] *Department of Psychiatry, University of Wisconsin-Madison, Madison, WI, USA*
[b] *Neuroscience Training Program, University of Wisconsin-Madison, Madison, WI, USA*
[c] *Medical Scientist Training Program, University of Wisconsin-Madison, Madison, WI, USA*
[d] *Department of Neurological Surgery, University of Wisconsin-Madison, Madison, WI, USA*

ARTICLE INFO

ABSTRACT

The ventromedial prefrontal cortex (vmPFC) plays a key role in modulating emotional responses, yet the precise neural mechanisms underlying this function remain unclear. vmPFC interacts with a number of subcortical structures involved in affective processing, including the amygdala, hypothalamus, periaqueductal gray, ventral striatum, and bed nucleus of stria terminalis (BNST). While a previous study of non-human primates shows that vmPFC lesions reduce BNST activity and anxious behavior, no such causal evidence exists in humans. In this study, we used a novel application of magnetic resonance imaging (MRI) in neurosurgical patients with focal, bilateral vmPFC damage to determine whether vmPFC is indeed critical for modulating BNST function in humans. Relative to neurologically healthy subjects, who exhibited robust rest-state functional connectivity between vmPFC and BNST, the vmPFC lesion patients had significantly lower resting-state perfusion of the right BNST. No such perfusion differences were observed for the amygdala, striatum, hypothalamus, or periaqueductal gray. This study thus provides unique data on the relationship between vmPFC and BNST, suggesting that vmPFC serves to promote BNST activity in humans. This finding is relevant for neural circuitry models of mood and anxiety disorders.

1. Introduction

The ventromedial prefrontal cortex (vmPFC) plays a critical role in human social and affective processing. Dysfunction in this brain area is thought to be a key neural substrate underlying the pathophysiology of mood and anxiety disorders (Critchley, Mathias, & Dolan, 2001; Drevets, Price, & Furey, 2008; Milad, Rauch, Pitman, & Quirk, 2006; Myers-Schulz &

Koenigs, 2012; Price, 1999). However, the precise mechanisms by which vmPFC dysfunction contributes to affective psychopathology are not fully understood. A leading neural circuit model proposes that vmPFC serves to regulate negative affect via top-down inhibition of brain regions involved in processing negative emotion—particularly the amygdala—and that pathologically elevated levels of negative affect in mood and anxiety disorders result from deficient vmPFC-mediated inhibition of amygdala activity (Milad et al., 2006; Quirk & Gehlert, 2003; Rauch, Shin, & Phelps, 2006). While this model is consistent with a considerable body of anatomical, behavioral, and neurophysiological data from rodent fear conditioning paradigms (Milad et al., 2006), studies of human lesion patients suggest a more complex role of vmPFC in affective function. For instance, although vmPFC lesion patients exhibit increased amygdala activity in response to aversive stimuli (Motzkin et al., 2015), vmPFC damage has been shown to *reduce* the likelihood of developing PTSD and depression (Koenigs, Huey, Calamia, et al., 2008; Koenigs, Huey, Raymont, et al., 2008). These findings suggest that vmPFC may coordinate multiple neural processes critical for the expression of negative affect in humans. Beyond top-down inhibition of amygdala, vmPFC may also modulate activity in other regions, such as the bed nucleus of the stria terminalis (BNST).

The BNST is a basal forebrain structure that is considered to be a component of the "extended amygdala" complex, in light of similarities in development, connectivity, and cytoarchitecture to the adjacent central nucleus of the amygdala (Heimer, Harlan, Alheid, Garcia, & de Olmos, 1997). The BNST and vmPFC are strongly interconnected (Avery et al., 2014), and BNST activity has been linked to anxiety-related behavior (Davis & Whalen, 2001; Kalin, Shelton, Fox, Oakes, & Davidson, 2005; Mobbs et al., 2010; Somerville,

Wagner, et al., 2013; Somerville, Whalen, & Kelley, 2010; Straube, Mentzel, & Miltner, 2007; Walker, Toufexis, & Davis, 2003). Moreover, a previous neuroimaging study in non-human primates found that bilateral orbitofrontal cortex (OFC) lesions (which included regions of vmPFC) were associated with reduced BNST metabolism and reduced anxious behavior in a human intruder paradigm (Fox et al., 2010; Kalin, Shelton, & Davidson, 2007). In addition, across the lesioned and non-lesioned monkeys, the level of BNST metabolism positively correlated with the degree of anxious behavior. These findings suggest that vmPFC/OFC may play a crucial role in generating or maintaining negative affect by promoting BNST activity. To explore this hypothesis in humans, we employed a magnetic resonance imaging (MRI) measure of resting cerebral blood flow (CBF) in a sample of neurosurgical patients with circumscribed bilateral vmPFC lesions. We hypothesized that, consistent with the results of the non-human primate study (Fox et al., 2010), humans with bilateral vmPFC damage would exhibit reduced BNST blood perfusion, which would in turn correlate with self-report measures of negative affect and anxiety. Furthermore, we used rest-state fMRI in the healthy adult comparison group to assess functional connectivity between BNST and vmPFC.

2.   Methods

2.1.   Participants

The lesion group consisted of four adult neurosurgical patients with extensive bilateral parenchymal damage, largely confined to the vmPFC—defined as the medial one-third of the orbital surface and the ventral one-third of the medial surface of prefrontal cortex, bilaterally (Fig. 1). Each of the four
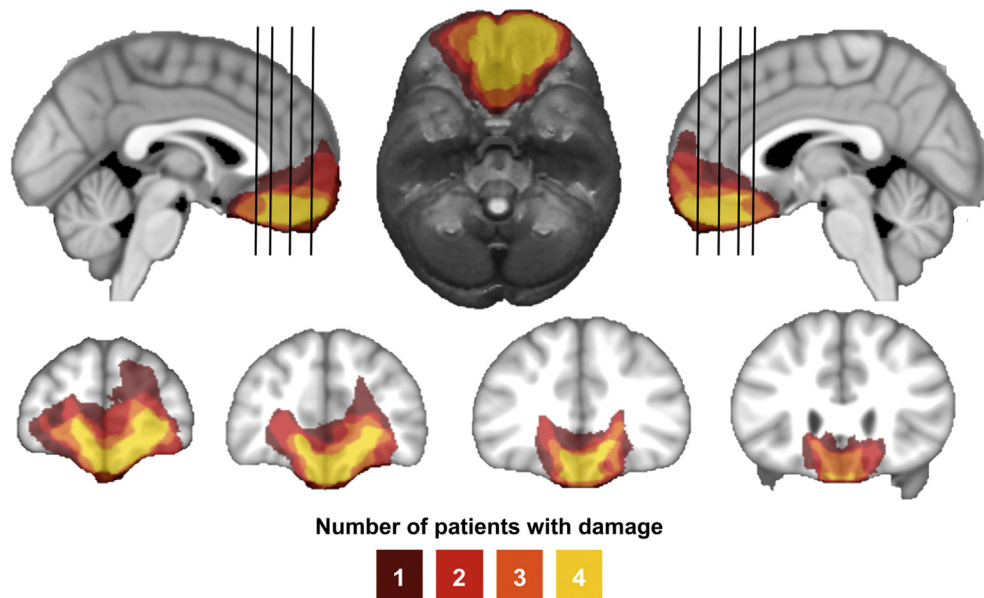

Number of patients with damage

| 1 | 2 | 3 | 4 |

Fig. 1 − Lesion overlap of vmPFC patients. Color indicates the number of overlapping lesions at each voxel. All vmPFC patients had damage to the medial one-third of the OFC and the ventral one-third of medial surface of prefrontal cortex, bilaterally. This area includes Brodmann areas 11, 12, 24, 25, 32, and the medial portion of 10 below the level of the genu of the corpus callosum, as well as subjacent white matter.

patients underwent surgical resection of a large anterior cranial fossa meningioma via craniotomy. Initial clinical presentations included subtle or obvious personality changes over several months preceding surgery. On post-surgical MRI, although vasogenic edema largely resolved, there were persistent T_2-weighted signal changes, consistent with gliosis, in the vmPFC bilaterally. All experimental procedures were conducted more than three months after surgery, when the expected recovery was complete. At the time of testing, all patients had focal, stable MRI signal changes and resection cavities and were free of dementia and substance abuse. Nineteen healthy adults with no history of brain injury, neurological or psychiatric illness, or current use of psychoactive medication were recruited as a normal comparison (NC) group. Demographic and neuropsychological data for the vmPFC and NC groups are summarized in Table 1.

2.2. MRI data acquisition

All structural and functional MRI data were acquired using a 3.0 T GE Discovery MR750 scanner equipped with an 8-channel radio-frequency head coil array (General Electric Medical Systems; Waukesha, WI). High-resolution T_1-weighted anatomical images were acquired using an inversion-recovery spoiled GRASS [SPGR] sequence (TR = 8.2 msec, TE = 3.2 msec, $\alpha = 12°$, FOV = 256 × 256 mm, matrix = 256 × 256, in-plane resolution = 1 × 1 mm^2, slice thickness = 1 mm, 1024 axial slices). To facilitate lesion segmentation, we collected a separate T_2-weighted FLAIR scan (TR = 8650 msec, TE = 136 msec, $\alpha = 0°$, FOV = 220 × 220 mm^2, matrix = 512 × 512, in-plane resolution = .43 × .43 mm^2, slice thickness = 5 mm, gap 1 mm, 25 axial slices).

Baseline resting CBF was estimated using a 3D fast spin echo spiral sequence with pseudocontinuous arterial spin labeling (pcASL) (Dai, Garcia, de Bazelaire, & Alsop, 2008; Okonkwo et al., 2014; Xu et al., 2010) and background suppression for quantitative perfusion measurements (TR = 4653 msec, TE = 10.5 msec, post-labeling delay = 1525 msec, labeling duration = 1450 msec, eight interleaved spiral arms with 512 samples at 62.5 kHz bandwidth and 38 4-mm thick slices, number of excitations = 3, scan duration = 4.5 min).

Whole-brain functional scans were acquired using a T_2*-weighted gradient-echo echoplanar imaging (EPI) sequence (TR = 2000 msec; TE = 22 msec; $\alpha = 79°$; FOV = 224 × 224 mm^2; matrix = 64 × 64, in-plane resolution = 3.5 × 3.5 mm^2, slice

thickness = 3 mm, gap = .5 mm, 38 interleaved axial oblique slices). Field maps were acquired using two separate acquisitions (TR = 600 msec, TE_1 = 7 msec, TE_2 = 10 msec, $\alpha = 60°$, FOV = 240 × 240 mm^2, matrix = 256 × 128, slice thickness = 4 mm, 33 axial oblique slices). Rest-state functional images were collected while subjects lay still and awake, passively viewing a fixation cross for 5 min. Scans were acquired in the following order: pcASL, field map, rest, task, T1, T2-FLAIR. The fMRI task data from this scan session are presented in separate manuscripts (Motzkin et al., 2014, 2015).

2.3. Lesion segmentation and image normalization

Individual vmPFC lesions were visually identified and manually segmented on the T_1-weighted images. Lesion boundaries were drawn to include areas with gross tissue damage or abnormal signal characteristics on T_1 or T_2 FLAIR images. T_1-weighted images were skull-stripped, rigidly co-registered with a functional volume from each subject, then diffeomorphically aligned to the Montreal Neurological Institute (MNI) coordinate system using a Symmetric Normalization (SyN) algorithm (Avants & Gee, 2004) with constrained cost-function masking to prevent warping of tissue within the lesion mask (Brett, Leff, Rorden, & Ashburner, 2001). We created the lesion overlap map (Fig. 1) by computing the sum of aligned binary lesion masks for all four vmPFC patients.

2.4. Cerebral perfusion analysis

Quantitative CBF images from pcASL were rigidly co-registered with a T_2*-weighted EPI volume from the task scan and normalized to MNI space. Normalized CBF volumes were scaled to whole-brain CBF (after masking out the lesion in vmPFC patients) and smoothed with a 6 mm full-width at half-maximum (FWHM) Gaussian kernel. To test the main study hypothesis, we used regions-of-interest (ROIs) corresponding to the right and left BNST (Fig. 2). BNST ROIs were hand-drawn on the MNI template brain using neuroanatomical boundaries from the human brain atlas of Mai (Mai, Assheuer, & Paxinos, 2003). Comparing the field map data between groups, we found no significant differences in signal distortion or dropout in the region of BNST (Supplementary Fig. 1). To determine the specificity of between-group differences, we also examined group differences in mean unscaled whole-brain CBF, as well as differences in scaled CBF for additional subcortical ROIs that

Table 1 — Subject characteristics.

	Age	Sex	Edu	IQ	Pos Aff	Neg Aff	BDI-II	STAI-T
vmPFC (n = 4)	58.5 (6.2)	3 M 1 F	15.5 (4.1)	103.8 (12.4)	36 (8.4)	17.0 (8.7)	7.0 (3.2)	34.3 (9.5)
NC (n = 19)	51.7 (9.9)	11 M 8 F	17.7 (3.5)	110.9 (7.2)	37.8 (4.9)	13.0 (2.4)	4.0 (3.3)	31.6 (6.0)
p (vmPFC vs NC)	.16	.63	.51	.25	.56	.73	.11	.44

Means are presented with standard deviations in parentheses. Edu, years of education; IQ, intelligence quotient estimated by the Wide Range Achievement Test 4, Blue Reading subtest (Wilkinson & Robertson, 2006); Pos/Neg Aff, scores from the Positive and Negative Affect Schedule (PANAS) (Watson et al., 1988); BDI-II, Beck Depression Inventory-II (Beck et al., 1996); STAI-T, trait version of the Spielberger State Trait Anxiety Inventory (Spielberger et al., 1983).
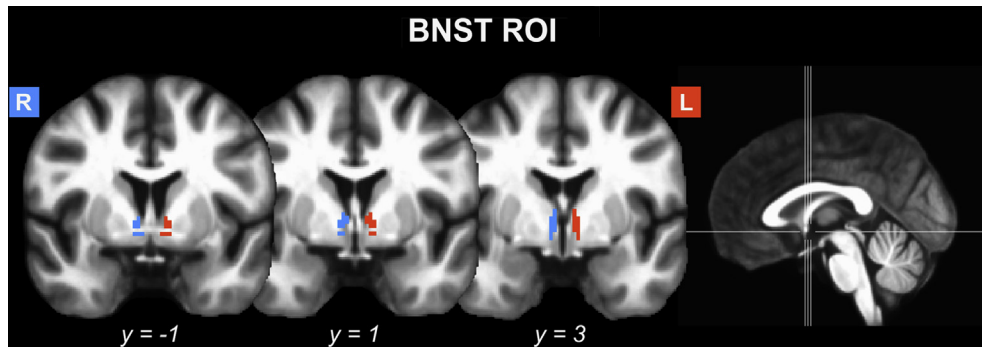
Fig. 2 — BNST ROIs. Right (blue) and left (orange) BNST ROIs used to examine group differences in perfusion.

are known to be directly connected with vmPFC (amygdala, mediodorsal nucleus of the thalamus, hypothalamus, periaqueductal gray, and ventral striatum) as well as for several subcortical areas not densely or directly connected with vmPFC (lateral geniculate nucleus, caudate nucleus, putamen). Mediodorsal thalamus, hypothalamus, and lateral geniculate nucleus ROIs were generated using Talairach atlas labels from AFNI's built-in Talairach Daemon (Talairach & Tournoux, 1988). Striatal ROIs (ventral striatum, caudate nucleus, and putamen) were generated using spheres with a radius of 3.5 mm centered on coordinates corresponding to the inferior ventral striatum, dorsal caudate, and dorsal rostral putamen ROIs reported in a previous functional connectivity study (Di Martino et al., 2008), which was based on a large-scale meta-analysis of striatal connectivity (Postuma & Dagher, 2006). The periaqueductal gray ROI was hand-drawn in MRIcron software on the group average anatomical volume in MNI template space, based on neuroanatomical boundaries from the human brain atlas of Mai (Mai et al., 2003). All between-group comparisons were assessed using non-parametric Mann−Whitney−Wilcoxon tests.

2.5.   fMRI preprocessing and analysis

Rest-state fMRI data analysis was performed using AFNI (Cox, 1996) and FSL (http://www.fmirb.ox.ac.uk/fsl/). EPI volumes were slice time corrected using the first slice as a reference (sequential acquisition, Fourier interpolation), field map corrected (Jezzard & Clare, 1999), and motion corrected by rigid body alignment to the first EPI acquisition. Next, images were deobliqued and the first three volumes were omitted from the EPI time series. Data were then motion corrected (3dvolreg) and despiked to remove extreme time series outliers. Finally, the time series data were band-pass filtered (.01 < f < .1) and spatially smoothed with a 4 mm FWHM Gaussian kernel. Two NC subjects were excluded from the rest-state analysis ($n = 1$ with excessive head motion >2 mm (Power, Barnes, Snyder, Schlaggar, & Petersen, 2012), $n = 1$ due to errors in field map correction) for a total sample size of $n = 17$ NC subjects. Functional connectivity was assessed using the hand-drawn anatomical ROIs in right and left BNST as seeds. Functional connectivity was computed using a GLM with the mean resting-state BOLD time series extracted from each subject-specific ROI and eight regressors of no interest, including six motion covariates, and average time series from white matter and ventricles. To further control for subject motion, volumes in which more than 10% of voxels were time series outliers were censored in the GLM. Correlation coefficients were converted to z-scores via Fisher's r-to-z transform and corrected for degrees of freedom. Resulting z-score maps were aligned to MNI space and resampled to 3 mm^3 isotropic resolution for subsequent second-level analyses.

To specifically examine whether the BNST ROIs used in this study exhibited significant functional connectivity with vmPFC in the NC group, we conducted a whole brain voxel-wise one-sample t-test against zero using z-transformed BNST connectivity maps from each subject. Group differences in right and left BNST functional connectivity were assessing using whole-brain voxel-wise two-sample t-tests. All statistical maps were FWE-corrected for multiple comparisons across the whole brain at the cluster level ($p_{FWE} < .05$), using a height threshold of $p < .001$ (Forman et al., 1995; Carp, 2012). A corrected $p_{FWE} < .05$ was achieved using a cluster extent threshold of 37 voxels (999 mm^3), calculated using Monte Carlo simulations.

2.6.   Relationship to anxiety measures

To investigate whether individual differences in anxiety were related to CBF in BNST, we regressed self-report measures of negative affect and anxiety on CBF values in BNST ROIs. Self-report scales were validated measures of trait anxiety (STAI-T) (Spielberger, Gorsuch, Lushene, Vagg, & Jacobs, 1983), depression (BDI) (Beck, Steer, & Brown, 1996), and negative affect (PANAS-negative) (Watson, Clark, & Tellegen, 1988). Two separate linear regression models were conducted for each measure, one examining the strength of the relationship in the NC group alone, and a second examining the relationship across both the NC and vmPFC groups together. Regression analyses were considered significant at $p < .05$.

3.   Results

The vmPFC lesion patients exhibited significantly lower perfusion in the right BNST, as compared to NC subjects

Table 2 — ASL cerebral perfusion data.

ROI	NC mean	NC SD.	vmPFC mean	vmPFC SD.	W	p
Whole brain	36.30	8.73	40.09	13.65	31	.611
BNST						
L BNST	1.07	.14	1.00	.16	50	.366
R BNST	1.03	.16	.83	.07	65	.027
vmPFC network						
L amygdala	1.11	.15	1.23	.11	20	.162
R amygdala	1.1	.15	1.01	.19	46	.557
L ventral striatum	1.43	.21	1.31	.13	51	.324
R ventral striatum	1.36	.23	1.14	.07	58	.116
L MD thalamus	1.28	.09	1.23	.05	51	.324
R MD thalamus	1.32	.10	1.11	.10	72	.003
L hypothalamus	1.08	.16	1.01	.09	46	.557
R hypothalamus	1.07	.18	.91	.04	61	.067
Periaqueductal gray	.94	.12	.96	.11	33	.725
Non-vmPFC network						
L caudate	1.24	.21	1.17	.23	45	.611
R caudate	1.29	.22	1.18	.14	52	.286
L putamen	1.26	.23	1.26	.17	36	.907
R putamen	1.32	.23	1.27	.18	42	.785
LGN thalamus	1.04	.17	1.08	.08	28	.456
R LGN thalamus	1.14	.22	1.03	.09	50	.366

Significant group differences are in italics. L, left; R, right; BNST, bed nucleus of stria terminalis; LGN, lateral geniculate nucleus; MD, mediodorsal.

($W = 65$, $p = .027$), supporting the hypothesis that vmPFC plays a critical role in promoting BNST function. There was no significant difference between groups for the left BNST ($W = 50$, $p = .37$). Among the comparison ROIs, the groups differed in only one region—the right mediodorsal nucleus of the thalamus ($W = 72$, $p = .003$). This unpredicted result survives Bonferroni correction for the total number of comparison ROIs ($\alpha = .05/13 = .004$). Complete group ASL results are presented in Table 2. BNST ASL data for each individual subject are presented in Supplementary Fig. 2.

To further explore the observed effect of vmPFC damage on BNST blood flow, we used rest-state fMRI to determine whether the BNST ROI used in this study is functionally connected with the vmPFC among the neurologically healthy subjects. As expected, the NC subjects exhibited significant rest-state functional connectivity between the right BNST and a single 116-voxel cluster within the vmPFC (Fig. 3).

Importantly, the region of significant BNST functional connectivity was located in an area in which all four vmPFC patients had substantial damage. The left BNST seed exhibited a similar pattern of rest-state connectivity in the NC group, demonstrating significantly correlated activity in two clusters (45 and 91 voxels) located within the vmPFC. In a follow-up analysis examining group differences in functional connectivity, we observed no significant group differences in right BNST connectivity with any region outside of the area damaged in the vmPFC group. We did not specifically assess functional connectivity between the BNST and vmPFC in the lesion group because all four patients had significant damage to this region.

There were no significant relationships between any of the three self-reported measures of negative affect (BDI, STAI, and PANAS) and right or left BNST CBF, either within the NC group or across the full sample (all p's > .10).
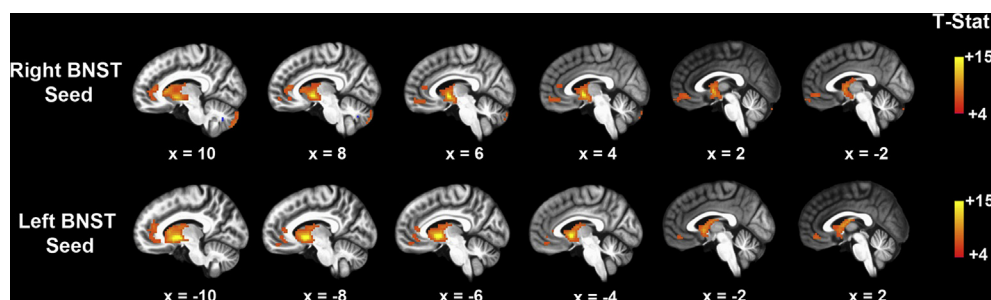

Fig. 3 — Rest-state functional connectivity for the right and left BNST ROI in $n = 17$ NC subjects. Significant functional connectivity was observed between the right BNST and a region of vmPFC in which all four vmPFC patients had damage (top row). A similar pattern of functional connectivity with the vmPFC was found for the left BNST ROI (bottom row). Coordinates presented (in mm) in MNI template space, thresholded at $p_{\mathrm{FWE}} < .05$.

4. Discussion

In this study, we demonstrate a significant and rather selective reduction in right BNST perfusion in patients with bilateral vmPFC lesions. This finding supports our primary hypothesis, which was based on a non-human primate combined PET/lesion study, demonstrating reduced BNST metabolism following bilateral OFC lesions (Fox et al., 2010). Our study is the first to use quantitative neuroimaging in human lesion patients to show an effect of vmPFC damage on resting cerebral perfusion, thereby providing unique and novel data regarding the causal relationship between vmPFC and BNST. More specifically, our data suggest that vmPFC normally serves to promote BNST activity, which in turn could enhance behavioral and physiological components of negative emotion (Davis & Shi, 1999; Walker et al., 2003). This vmPFC-BNST interaction could explain in part why vmPFC damage in humans has been associated with blunted affect (Barrash, Tranel, & Anderson, 2000), diminished physiological arousal to emotionally evocative stimuli (Damasio, Tranel, & Damasio, 1990), and a reduced likelihood of developing PTSD and depression (Koenigs, Huey, Calamia, et al., 2008; Koenigs, Huey, Raymont, et al., 2008). A putative interaction between vmPFC and BNST is supported by our functional connectivity analysis (Fig. 3) as well as by previous human neuroimaging data documenting robust functional and structural connections between the two regions (Avery et al., 2014). This vmPFC-BNST interaction could thus constitute an important addition to neural circuitry models of mood and anxiety disorders, which have predominantly focused on the role of vmPFC in inhibiting amygdala activity (Milad et al., 2006; Quirk & Gehlert, 2003; Rauch et al., 2006).

The model of vmPFC-BNST interaction proposed above is based largely on previous research linking BNST activity to the expression of trait-like anxiety (Davis & Whalen, 2001; Kalin et al., 2005; Walker et al., 2003). Unlike the amygdala, which has been implicated in rapid, time-limited fear responses consistent with orienting towards potentially threatening stimuli, BNST is thought to be involved in generating and maintaining responses consistent with sustained anxiety (Walker et al., 2003). Although direct axonal connections between vmPFC and BNST have not been well characterized in primates, high-resolution tracing studies in rodents have identified robust direct projections from infralimbic cortex—the putative homologue of human vmPFC—to BNST (McDonald, Shammah-Lagnado, Shi, & Davis, 1999), in addition to well-documented indirect connections through other limbic regions like the amygdala, insula, and mediodorsal thalamic nucleus (Dong, Petrovich, & Swanson, 2001; Dong, Petrovich, Watts, et al., 2001; McDonald et al., 1999). Each of these areas in turn project to brainstem and hypothalamic nuclei involved in coordinating peripheral aspects of an emotional response (Heimer et al., 1997; Jennings et al., 2013; Tye et al., 2011). Together, these regions form a network well-suited for the modulation and expression of behavioral and physiological components of emotion.

Unlike the previous lesion study in non-human primates (Fox et al., 2010), we did not observe a significant relationship between BNST perfusion and measures of anxiety. There are several potential explanations for this null finding. One is that the ASL perfusion measure employed here may be too coarse of an index of BNST activity to correlate with specific aspects of emotional experience. Recent evidence indicates that BNST consists of distinct subregions with divergent roles in emotional expression. A study in rodents using optogenetics to activate and deactivate discrete sub-populations of BNST neurons found that focal stimulation of adjacent BNST subregions elicited opposing anxiolytic and anxiogenic effects (Jennings et al., 2013; Kim et al., 2013). Thus, the lack of an association between BNST perfusion and anxiety in the present may study reflect the conflicting effects of changes in blood flow on anatomically distinct and functionally antagonistic regions of BNST. Secondly, given that previous associations between BNST metabolism and anxiety phenotypes were observed using PET scanning under conditions designed to elicit anxious responses (Fox et al., 2010; Kalin et al., 2005), our approach of examining resting blood flow inside the MRI environment (with no anxiety-inducing stimulus) may be sufficient to detect overall differences in CBF that results from vmPFC damage, but not sensitive enough to observe the expected relationships between BNST function and anxious behavior. Finally, there was a narrow range of self-reported negative affect in our healthy adult comparison sample. All subjects were well within the subclinical range (Beck et al., 1996; Spielberger et al., 1983; Watson et al., 1988), which may have limited our ability to detect a correlation between individual differences in BNST perfusion and self-reported anxiety. Future work in larger samples using more robust emotion induction paradigms and a broader range of anxiety levels will be necessary to more fully elucidate the relationship between BNST activity and psychopathology.

Several additional findings warrant further consideration. One is the unpredicted effect of vmPFC damage on mediodorsal thalamus perfusion. Among all comparison ROIs, only the right mediodorsal thalamus exhibited a significant group difference. This finding can likely be explained by the fact that the mediodorsal nucleus is the region of thalamus that is the most densely interconnected with vmPFC (Ongur & Price, 2000). However, it is important to note that not all regions that are densely interconnected with vmPFC exhibited reductions in perfusion; no significant group differences were observed in either hemisphere for amygdala, ventral striatum, hypothalamus, or periaqueductal gray. This pattern of results suggests that vmPFC may play an especially critical role in modulating the activity of BNST and mediodorsal thalamus. Alternatively, the lack of significant findings in other brain regions could be due the small sample of vmPFC lesion patients, though the primate PET study also found no significant effect of OFC damage on amygdala metabolism (Fox et al., 2010). Another noteworthy finding is that the significant reductions in BNST and mediodorsal thalamus perfusion were observed only in the right hemisphere. Even in a follow-up analysis, in which we refined our BNST ROI based on statistically significant ($p < .005$) functional connectivity with the region of vmPFC exhibiting maximal overlap in the patient group, we see a similar result: vmPFC lesion patients had significantly lower perfusion in right BNST ($W = 64$; $p = .035$), whereas there was no

significant group difference in left BNST ($W = 48$; $p = .46$). These lateralized effects may be due to the lesion characteristics of our vmPFC patient sample. Although all patients' lesions involved significant bilateral damage to vmPFC, each patient had slightly greater damage on the right side. Another possibility is that there may be some degree of asymmetry in the structure and function of the BNST. For example, fMRI studies have shown unilateral activation of BNST in anxiety-inducing paradigms (Somerville, Whalen, & Kelley, 2010; Somerville, Wagner, et al., 2013; Straube et al., 2007). Moreover, consistent with our findings, the PET study of non-human primates with bilateral OFC lesions reported a significant reduction in the metabolism of right, but not left, BNST (Fox et al., 2010). Future work in larger patient samples with more heterogeneous vmPFC lesions could more conclusively determine the link between lateralization of vmPFC damage and BNST perfusion.

The sample size of vmPFC lesion patients was somewhat limited ($n = 4$). For this study, we employed extremely stringent selection criteria for our target group; lesions had to involve substantial portions of vmPFC bilaterally, but could not extend significantly outside vmPFC. Furthermore, because the study involved fMRI, we could not include patients with metallic implants, such as aneurysm clips. To meet these criteria, we selected a group of patients who had all undergone surgical resection of large orbital meningiomas. So, although our sample size may be small by conventional vmPFC lesion patient standards (which typically feature $n = 5$ to $n = 12$ vmPFC lesion patients), it is unique with respect to the homogeneity of etiology, uniformity and selectivity of bilateral vmPFC lesions, and compatibility with MRI.

One limitation of the present study is the single neuroimaging measure (ASL) used to index BNST activity. Because resting CBF is tightly coupled to cerebral metabolism (Fox & Raichle, 1986), ASL can be interpreted as a proxy measure of cerebral metabolism—and hence underlying neural activity—similar to PET (Okonkwo et al., 2014; Xu et al., 2010). However, the ASL data in this study only indicate resting state perfusion. Future fMRI studies could build upon the present results by determining whether vmPFC damage also diminishes stimulus-evoked BNST activity in anxiogenic tasks (Alvarez, Chen, Bodurka, Kaplan, & Grillon, 2011; Grupe, Oathes, & Nitschke, 2013; Somerville et al., 2013).

In sum, through a unique application of ASL cerebral perfusion imaging in patients with bilateral vmPFC lesions, we have demonstrated a role for vmPFC in promoting BNST function. This finding corroborates non-human primate data and yields novel insight on the brain circuitry underlying human emotion. Future work will be needed to more fully elucidate the role of vmPFC in the modulation of BNST function, as this circuit may be central to the dysregulated affect associated with anxious psychopathology.

Funding

Conflicts of interest

The authors declare no potential conflicts of interest.

Supplementary data

REFERENCES

Alvarez, R. P., Chen, G., Bodurka, J., Kaplan, R., & Grillon, C. (2011). Phasic and sustained fear in humans elicits distinct patterns of brain activity. *NeuroImage, 55*(1), 389–400.

Avants, B., & Gee, J. C. (2004). Geodesic estimation for large deformation anatomical shape averaging and interpolation. *NeuroImage, 23*(Suppl. 1), S139–S150.

Avery, S. N., Clauss, J. A., Winder, D. G., Woodward, N., Heckers, S., & Blackford, J. U. (2014). BNST neurocircuitry in humans. *NeuroImage, 91C*, 311–323.

Barrash, J., Tranel, D., & Anderson, S. W. (2000). Acquired personality disturbances associated with bilateral damage to the ventromedial prefrontal region. *Developmental Neuropsychology, 18*(3), 355–381.

Beck, A. T., Steer, R. A., & Brown, G. K. (1996). *Manual for the beck depression inventory-II*. San Antonio, TX: Psychological Corporation.

Brett, M., Leff, A. P., Rorden, C., & Ashburner, J. (2001). Spatial normalization of brain images with focal lesions using cost function masking. *NeuroImage, 14*(2), 486–500.

Carp, J. (2012). The secret lives of experiments: methods reporting in the fMRI literature. *NeuroImage, 63*(1), 289–300.

Critchley, H. D., Mathias, C. J., & Dolan, R. J. (2001). Neural activity in the human brain relating to uncertainty and arousal during anticipation. *Neuron, 29*(2), 537–545.

Dai, W., Garcia, D., de Bazelaire, C., & Alsop, D. C. (2008). Continuous flow-driven inversion for arterial spin labeling using pulsed radio frequency and gradient fields. *Magnetic Resonance in Medicine: Official Journal of the Society of Magnetic Resonance in Medicine/Society of Magnetic Resonance in Medicine, 60*(6), 1488–1497.

Damasio, A. R., Tranel, D., & Damasio, H. (1990). Individuals with sociopathic behavior caused by frontal damage fail to respond autonomically to social stimuli. *Behavioural Brain Research, 41*(2), 81–94.

Davis, M., & Shi, C. (1999). The extended amygdala: are the central nucleus of the amygdala and the bed nucleus of the stria terminalis differentially involved in fear versus anxiety? *Annals of the New York Academy of Sciences, 877*, 281–291.

Davis, M., & Whalen, P. J. (2001). The amygdala: vigilance and emotion. *Molecular Psychiatry, 6*(1), 13–34.

Di Martino, A., Scheres, A., Margulies, D. S., Kelly, A. M., Uddin, L. Q., Shehzad, Z., et al. (2008). Functional connectivity of human striatum: a resting state FMRI study. *Cerebral Cortex, 18*(12), 2735–2747.

Dong, H. W., Petrovich, G. D., & Swanson, L. W. (2001). Topography of projections from amygdala to bed nuclei of the stria terminalis. *Brain Research Reviews, 38*(1–2), 192–246.

Dong, H. W., Petrovich, G. D., Watts, A. G., & Swanson, L. W. (2001). Basic organization of projections from the oval and fusiform nuclei of the bed nuclei of the stria terminalis in adult rat brain. *Journal of Comparative Neurology, 436*(4), 430–455.

Drevets, W. C., Price, J. L., & Furey, M. L. (2008). Brain structural and functional abnormalities in mood disorders: implications for neurocircuitry models of depression. *Brain Structure & Function, 213*(1—2), 93—118.

Forman, S. D., Cohen, J. D., Fitzgerald, M., Eddy, W. F., Mintun, M. A., & Noll, D. C. (1995). Improved assessment of significant activation in functional magnetic resonance imaging (fMRI): use of a cluster-size threshold. *Magnetic Resonance in Medicine, 33*(5), 636—647.

Fox, P. T., & Raichle, M. E. (1986). Focal physiological uncoupling of cerebral blood flow and oxidative metabolism during somatosensory stimulation in human subjects. *Proceedings of the National Academy of Sciences of the United States of America, 83*(4), 1140—1144.

Fox, A. S., Shelton, S. E., Oakes, T. R., Converse, A. K., Davidson, R. J., & Kalin, N. H. (2010). Orbitofrontal cortex lesions alter anxiety-related activity in the primate bed nucleus of stria terminalis. *Journal of Neuroscience, 30*(20), 7023—7027.

Grupe, D. W., Oathes, D. J., & Nitschke, J. B. (2013). Dissecting the anticipation of aversion reveals dissociable neural networks. *Cerebral Cortex, 23*(8), 1874—1883.

Heimer, L., Harlan, R. E., Alheid, G. F., Garcia, M. M., & de Olmos, J. (1997). Substantia innominata: a notion which impedes clinical-anatomical correlations in neuropsychiatric disorders. *Neuroscience, 76*(4), 957—1006.

Jennings, J. H., Sparta, D. R., Stamatakis, A. M., Ung, R. L., Pleil, K. E., Kash, T. L., et al. (2013). Distinct extended amygdala circuits for divergent motivational states. *Nature, 496*(7444), 224—228.

Jezzard, P., & Clare, S. (1999). Sources of distortion in functional MRI data. *Human Brain Mapping, 8*(2—3), 80—85.

Kalin, N. H., Shelton, S. E., & Davidson, R. J. (2007). Role of the primate orbitofrontal cortex in mediating anxious temperament. *Biological Psychiatry, 62*(10), 1134—1139.

Kalin, N. H., Shelton, S. E., Fox, A. S., Oakes, T. R., & Davidson, R. J. (2005). Brain regions associated with the expression and contextual regulation of anxiety in primates. *Biological Psychiatry, 58*(10), 796—804.

Kim, S. Y., Adhikari, A., Lee, S. Y., Marshel, J. H., Kim, C. K., Mallory, C. S., et al. (2013). Diverging neural pathways assemble a behavioural state from separable features in anxiety. *Nature, 496*(7444), 219—223.

Koenigs, M., Huey, E. D., Calamia, M., Raymont, V., Tranel, D., & Grafman, J. (2008). Distinct regions of prefrontal cortex mediate resistance and vulnerability to depression. *Journal of Neuroscience, 28*(47), 12341—12348.

Koenigs, M., Huey, E. D., Raymont, V., Cheon, B., Solomon, J., Wassermann, E. M., et al. (2008). Focal brain damage protects against post-traumatic stress disorder in combat veterans. *Nature Neuroscience, 11*(2), 232—237.

Mai, J. K., Assheuer, J., & Paxinos, G. (2003). *Atlas of the human brain* (2nd ed.). San Diego: Elsevier Academic Press.

McDonald, A. J., Shammah-Lagnado, S. J., Shi, C., & Davis, M. (1999). Cortical afferents to the extended amygdala. *Annals of the New York Academy of Sciences, 877*, 309—338.

Milad, M. R., Rauch, S. L., Pitman, R. K., & Quirk, G. J. (2006). Fear extinction in rats: implications for human brain imaging and anxiety disorders. *Biological Psychology, 73*(1), 61—71.

Mobbs, D., Yu, R., Rowe, J. B., Eich, H., FeldmanHall, O., & Dalgleish, T. (2010). Neural activity associated with monitoring the oscillating threat value of a tarantula. *Proceedings of the National Academy of Sciences of the United States of America, 107*(47), 20582—20586.

Motzkin, J. C., Philippi, C. L., Wolf, R. C., Baskaya, M. K., & Koenigs, M. (2015). Ventromedial prefrontal cortex is critical for the regulation of amygdala activity in humans. *Biological Psychiatry, 77*(3), 276—284.

Motzkin, J. C., Philippi, C. L., Wolf, R. C., Baskaya, M. K., & Koenigs, M. (2014). Ventromedial prefrontal cortex lesions alter neural and physiological correlates of anticipation. *Journal of Neuroscience, 34*(31), 10430—10437.

Myers-Schulz, B., & Koenigs, M. (2012). Functional anatomy of ventromedial prefrontal cortex: implications for mood and anxiety disorders. *Molecular Psychiatry, 17*(2), 132—141.

Okonkwo, O. C., Xu, G., Oh, J. M., Dowling, N. M., Carlsson, C. M., Gallagher, C. L., et al. (2014). Cerebral blood flow is diminished in asymptomatic middle-aged adults with maternal history of Alzheimer's disease. *Cerebral Cortex, 24*(4), 978—988.

Ongur, D., & Price, J. L. (2000). The organization of networks within the orbital and medial prefrontal cortex of rats, monkeys and humans. *Cerebral Cortex, 10*(3), 206—219.

Postuma, R. B., & Dagher, A. (2006). Basal ganglia functional connectivity based on a meta-analysis of 126 positron emission tomography and functional magnetic resonance imaging publications. *Cerebral Cortex, 16*(10), 1508—1521.

Power, J. D., Barnes, K. A., Snyder, A. Z., Schlaggar, B. L., & Petersen, S. E. (2012). Spurious but systematic correlations in functional connectivity MRI networks arise from subject motion. *NeuroImage, 59*(3), 2142—2154.

Price, J. L. (1999). Prefrontal cortical networks related to visceral function and mood. *Annals of the New York Academy of Sciences, 877*, 383—396.

Quirk, G. J., & Gehlert, D. R. (2003). Inhibition of the amygdala: key to pathological states? *Annals of the New York Academy of Sciences, 985*, 263—272.

Rauch, S. L., Shin, L. M., & Phelps, E. A. (2006). Neurocircuitry models of posttraumatic stress disorder and extinction: human neuroimaging research — past, present, and future. *Biological Psychiatry, 60*(4), 376—382.

Somerville, L. H., Wagner, D. D., Wig, G. S., Moran, J. M., Whalen, P. J., & Kelley, W. M. (2013). Interactions between transient and sustained neural signals support the generation and regulation of anxious emotion. *Cerebral Cortex, 23*(1), 49—60.

Somerville, L. H., Whalen, P. J., & Kelley, W. M. (2010). Human bed nucleus of the stria terminalis indexes hypervigilant threat monitoring. *Biological Psychiatry, 68*(5), 416—424.

Spielberger, C. D., Gorsuch, R. L., Lushene, R., Vagg, P. R., & Jacobs, G. A. (1983). *Manual for the state-trait anxiety inventory*. Palo Alto, CA: Consulting Psychologists Press.

Straube, T., Mentzel, H. J., & Miltner, W. H. (2007). Waiting for spiders: brain activation during anticipatory anxiety in spider phobics. *NeuroImage, 37*(4), 1427—1436.

Talairach, J., & Tournoux, P. (1988). *Co-planar stereotaxic atlas of the human brain*. New York: Theime Medical.

Tye, K. M., Prakash, R., Kim, S. Y., Fenno, L. E., Grosenick, L., Zarabi, H., et al. (2011). Amygdala circuitry mediating reversible and bidirectional control of anxiety. *Nature, 471*(7338), 358—362.

Walker, D. L., Toufexis, D. J., & Davis, M. (2003). Role of the bed nucleus of the stria terminalis versus the amygdala in fear, stress, and anxiety. *European Journal of Pharmacology, 463*(1—3), 199—216.

Watson, D., Clark, L. A., & Tellegen, A. (1988). Development and validation of brief measures of positive and negative affect: the PANAS scales. *Journal of Personality and Social Psychology, 54*(6), 1063—1070.

Wilkinson, G. S., & Robertson, G. J. (2006). *WRAT4: Wide range achievement test*. Lutz, FL: Psychological Assessment Resources.

Xu, G., Rowley, H. A., Wu, G., Alsop, D. C., Shankaranarayanan, A., Dowling, M., et al. (2010). Reliability and precision of pseudo-continuous arterial spin labeling perfusion MRI on 3.0 T and comparison with 15O-water PET in elderly subjects at risk for Alzheimer's disease. *NMR in Biomedicine, 23*(3), 286—293.